Picrite sills and crystal-melt reactions in the Honningsvåg Intrusive Suite, northern Norway

CHRISTIAN TEGNER

Danish Lithosphere Centre, Øster Voldgade 10, 1350 København K, Denmark

AND

BRIAN ROBINS

Department of Geology, University of Bergen, 5007 Bergen, Norway

Abstract

Field relations in the upper part of Intrusion II of the Caledonian Honningsvåg Intrusive Suite show that some peridotite sheets transgress, and include *in situ* rafts of, the adjacent gabbroic cumulates. Modal and textural analyses of three olivine melagabbro sheets show non-cotectic mineral proportions that are likely to result from crystal-melt reactions. Discordant, replacive fingers and pipes of feldspathic peridotite along interfaces between peridotite and overlying olivine melagabbro also suggest crystal-melt reactions.

It is proposed that several picritic sills intruded porous gabbroic cumulates in the upper part of Intrusion II. Lateral *infiltration* of picritic magma led to crystal-melt reactions, mainly assimilation of plagioclase and precipitation of olivine, resulting in the formation of olivine melagabbro and peridotite sheets, and replacive fingers and pipes of feldspathic peridotite.

KEYWORDS: crystal-melt reactions, picrite, cumulates, sills, Honningsvåg, Norway.

Introduction

LAYERED intrusions consisting of alternating ultramafic and gabbroic cumulates, e.g. Rum, Bushveld and Muskox are commonly interpreted as having crystallized sequentially from multiple magma injections emplaced along the magma chamber floor (e.g. Wager and Brown, 1968; Huppert and Sparks, 1980; Irvine, 1980). Recent interpretations of the Rum Complex, however, suggest that some peridotite sheets may be intrusive sills emplaced into unconsolidated troctolites (Morse *et al.*, 1987; Renner and Palacz, 1987; Bédard *et al.*, 1988). Intrusion of ultrabasic magma into gabbroic cumulates, forming wehrlitic plugs and sills, has recently been documented in the Kap Edvard Holm Complex (Bernstein *et al.*, 1992; Tegner and Wilson, 1993) and in plutonic rocks of the ocean floor as recorded in ophiolites (e.g. Bédard, 1993; Benn and Laurent, 1987; Juteau *et al.*, 1988) and in drill cores from the East Pacific Rise and the Mid-Atlantic Ridge (Girardeau and Francheteau, 1993).

Intrusion II of the Honningsvåg Intrusive Suite, northern Norway (Fig. 1, see Fig. 1 of companion paper by Tegner *et al.*, this volume), shares many similarities with the Rum Complex. It contains a sequence of macrolayers of peridotite (ocC), troctolite (pocC), olivine gabbro (paoC) and gabbronorite (pahC) that has been subdivided into 12 cyclic units. In the cumulus terminology used here o = olivine; p = plagioclase; a = Ca-rich pyroxene; h = Ca-poor pyroxene; c = chromite; C = cumulate, and the cumulus minerals are listed in order of decreasing modal abundance. Robins *et al.* (1987) proposed that crystallization took place from large-scale double-diffusive layers that resulted from repeated magma injections emplaced along the chamber floor (Fig. 2*a*; hereafter referred to as the 'replenishment model'). This model assumes that the crystallization front was inclined and can thereby explain the formation of wedge-shaped macrolayers.

This paper presents new field observations, petrographic data and mineral chemistry from the upper part of Intrusion II (cyclic units 5–12). The

Mineralogical Magazine, February 1996, Vol. 60, pp. 53–66

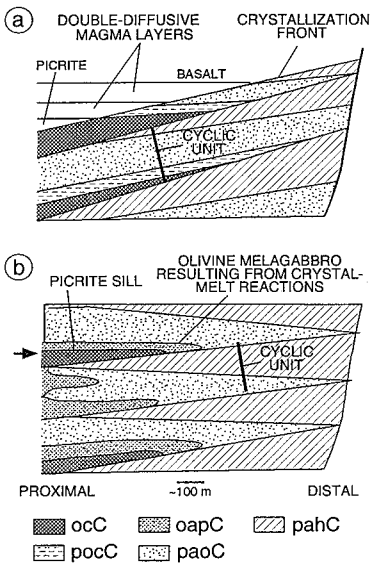

FIG. 2. Two alternative crystallization models. (*a*). Replenishment model of Robins *et al.* (1987). Crystallization from double-diffusive magma layers along a sloping crystallization front leads to the deposition of wedge-shaped macrolayers of ocC (peridotite), pocC (troctolite), paoC (olivine gabbro) and pahC (gabbro-norite). See text for explanation of the cumulus nomenclature. Addition of new magma at the base elevates pre-existing magma layers. This is recorded as cyclic units in the cumulate sequence. (*b*). Two-stage intrusive model proposed in this study. Unconsolidated paoC and pahC macrolayers exist prior to intrusion of picritic sills (Tegner *et al.*, this volume). Emplacement of intrusive picritic sills is initiated by lateral *infiltration* (from left to right on sketch) causing a conversion of paoC to oapC (olivine melagabbro) by crystal-melt reactions. Continuous supply of picritic magma leads to the development of a genuine sill, partly by infilling the space created by assimilation of the host, and partly by dilation. Crystallization of the sill itself results in ocC sheets.

presence of transgressive ocC, replacive cumulates and in some cases the stacking of macrolayers are difficult to explain satisfactorily with a replenishment model. An alternative model of two-stage intrusive magmatism (Fig. 2*b*) is therefore proposed. Magmatic replacement as a result of crystal-melt reactions is also discussed. This contribution is part of a recent investigation of the Honningsvåg Intrusive Suite. The data presented elsewhere (Tegner *et al.*, this volume) deal with the cumulates that existed prior to the picritic intrusions.

Field relations

Cyclic units of Intrusion II

Robins *et al.* (1987) classified cyclic units as: 'ideal' when macrolayers occurred in a systematic order as expected from phase relations (in this case from base to top: ocC, pocC, paoC, pahC); 'uncompleted' when one or more of the upper macrolayers are missing; 'reduced' when there is no ocC macrolayer at the base, and 'interrupted' when intermediary macrolayers are absent. Cyclic units showing ideal, incomplete and reduced macrolayer sequences may result from fractional crystallization following magma chamber replenishment. Interrupted macrolayer sequences are more difficult to explain because the sequence of cumulates diverges from that expected from the order of crystallization. Interrupted cyclic units have, however, been explained by the juxtaposition of compositionally distant double-diffusive magma layers (Robins *et al.*, 1987), and possibly by draining of magma back into the feeder zone (Robins *et al.*, 1991). Here we propose that in certain cases interrupted cumulate sequences may result from later intrusion of picritic sills.

Contact relations between ocC (peridotite) and surrounding rocks

In cyclic units 5–10 several wedge-shaped ocC sheets result in interrupted macrolayer sequences (Fig. 1). The two uppermost ocC sheets (up to ~20 m thick) clearly cut cumulates of cyclic units 8, 9 and 10 (Figs 1, 3*a*) while the rest are sub-concordant to modal layering of adjacent cumulates. Complex contact relations of the ocC sheet at the base of cyclic unit 7, however, suggest that these sub-concordant sheets also may intrude and/or replace the adjacent cumulates:

(1) Dm-thick peridotite layers, probably apophyses from the main ocC body, occur in places within the uppermost paoC of unit 6.

(2) The base of ocC may consist of alternating ocC and oapC (olivine melagabbro) layers; a cm-thick layer rich in Ca-rich pyroxene often occurs at the contact between the two rock-types (Fig. 4*e*).

(3) A <5 cm thick, persistent but discontinuous oapC layer rich in Ca-rich pyroxene (Fig. 3*d*) occurs ~8 m below the upper contact of the ocC; in places it can be followed for more than 200 m.

(4) Rafts and irregular blocks of *in situ* oapC (Figs. 3*b,c*, Fig. 5) occur within the uppermost metres of the ocC sheet.

(5) A 10–15 m thick transitional pocC sheet (in which the amount of olivine increases upwards) separates paoC of unit 6 from ocC of unit 7.

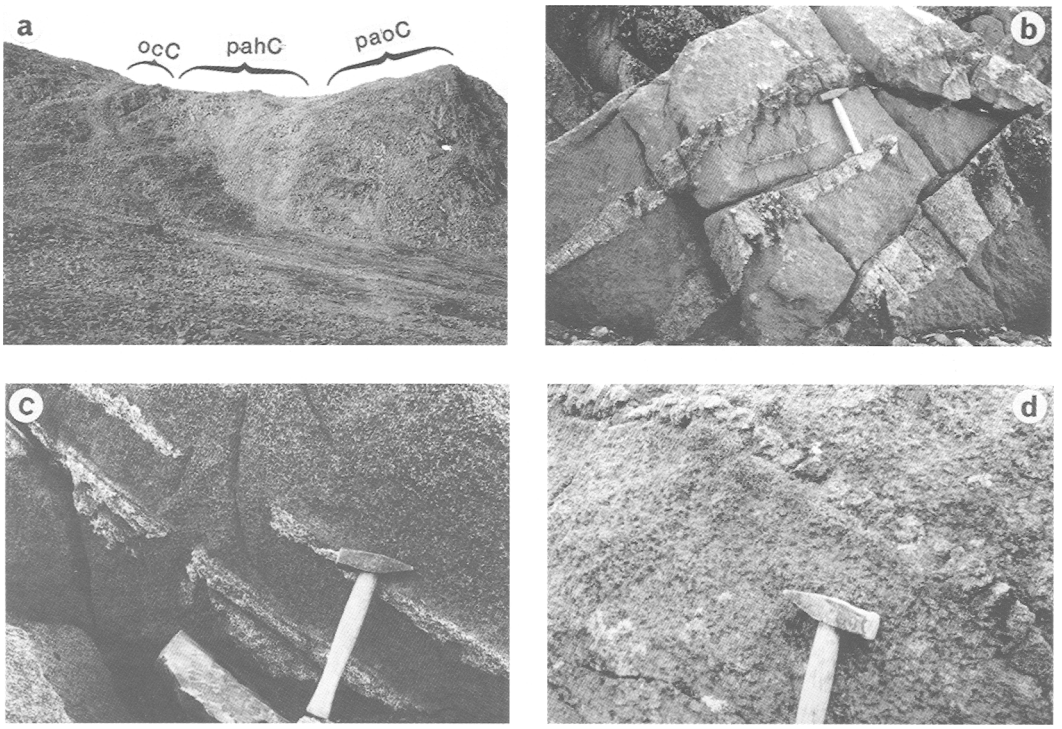

FIG. 3. Contact relations between ocC and adjacent cumulates. (*a*). Transgressive ocC (black) cutting pahC (light grey) of cyclic unit 8 at its north-eastern extreme. The flat foreground consist of Intrusion IV (see Fig. 1). Viewed from NE, width of photo is ~250 m. (*b*). ocC (dark) enclosing paoC rafts (light) in the north-eastern part of cyclic unit 5. (*c*). oapC rafts (light) occuring *in situ* in replacive peridotite (dark) ~2–3 m below the main ocC-oapC interface in cyclic unit 7. (*d*). Shows a thin oapC layer rich in Ca-rich pyroxene (diagonal from upper left to lower right) that is persistent for several hundred metres within the upper half of the ocC sheet in cyclic unit 7. The layer consists of segments with fairly flat tops and fingered bases, each separated by replacive peridotite fingers connecting ocC above and below the layer.

The oapC (olivine melagabbro) sheets

Three wedge-shaped oapC sheets (not recognized in former studies) occur in cyclic units 7 and 8 (Fig. 1). They are melanocratic with non-cotectic modal compositions (see below) and occur immediately above ocC within cyclic unit 7, within paoC of cyclic unit 7 and at the base of cyclic unit 8. The latter oapC sheet appears to pass into ocC towards the proximal parts of the intrusion.

Replacive feldspathic peridotite

Replacive bodies of feldspathic peridotite are ubiquitous over a strike length of ~1 km along the ocC/oapC contact within cyclic unit 7. The term 'replacive peridotite' is used for rocks forming transgressive pipes and fingers and is distinguished from ocC and oapC. The morphology of the pipes and fingers is highly variable (Figs. 4–6). The replacive nature is demonstrated by the non-matching sides of replacive peridotite bodies (which exclude simple intrusion of magma into dilational fractures) and by the lack of deformation or displacement of layering and lamination in the host.

The pipes are up to 0.5 m wide, often perpendicular to the overall interface, defined by the lack of cumulus plagioclase and penetrate up to 3 m into the overlying oapC. Outcrops allowing three-dimensional observations clearly demonstrate their sub-cylindrical nature in cross section. There is one large pipe (longer than 1 m) for every ~2 m along the contact (Fig. 5).

Petrography

Thin-sections from two representative localities in cyclic unit 7 (Fig. 6) have been prepared for a

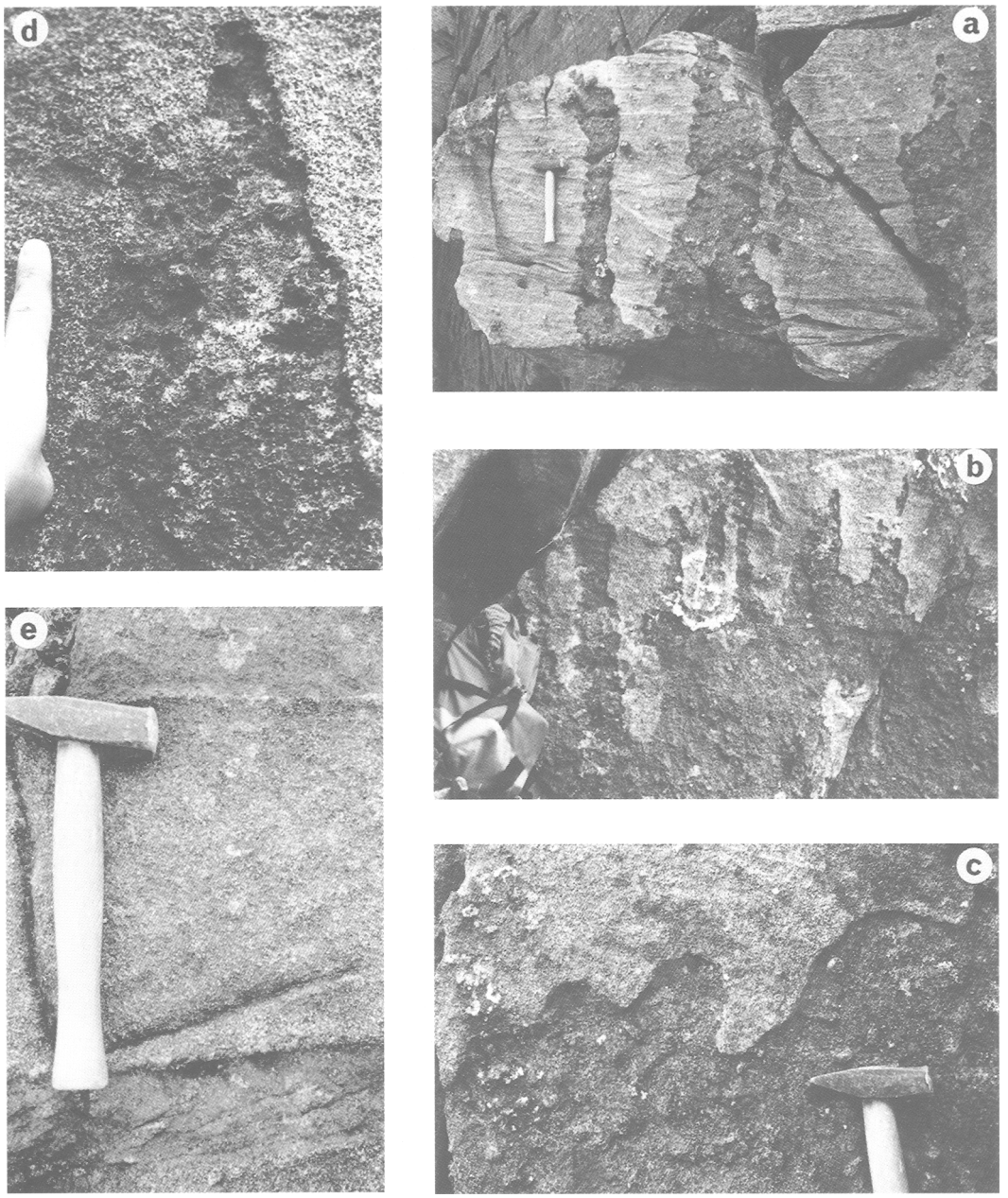

FIG. 4. *a–d*. Replacive fingers and pipes of feldspathic peridotite along the contact between ocC and overlying oapC in cyclic unit 7. Replacive peridotite forms low-relief, easily weathered, brownish, non-layered bodies crosscutting modally layered oapC. The contact is knife sharp and modal layering/lamination in the host is never deformed. Cm-sized Ca-poor pyroxene megacrysts in replacive peridotite causes a knotty appearance. Replacement bodies may have different shapes but upward tapering fingers and pipes sub-perpendicular to the overall contact are most common. (*e*). Alternating ocC and oapC (beneath hammer) layers in the basal part of the ocC sheet in cyclic unit 7. Note the cm-thick layers (resistant to weathering) enriched in Ca-rich pyroxene at the boundary between ocC and paoC.

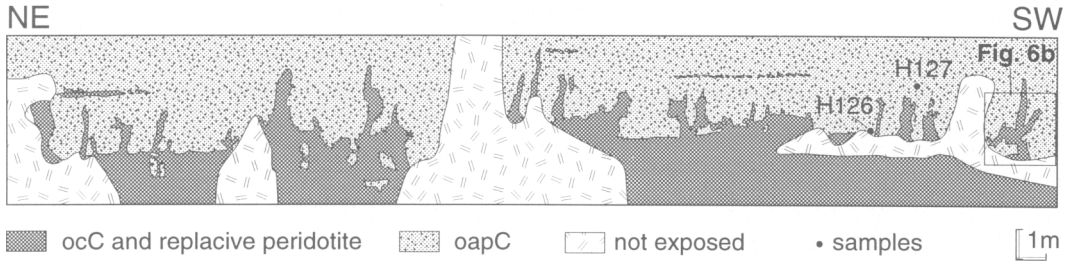

FIG. 5. Sketch showing the morphology of the contact in cyclic unit 7 between ocC and oapC in a ~30 m long exposure in the vicinity of profile 1 (see Fig. 1). The outcrop surface is generally sub-perpendicular to modal layering and therefore exposes a 'true' profile. Location of samples and locality shown in Fig. 6*b* are shown.

textural study and for mineral chemistry studies. Typical textures are shown in Fig. 7 and modal analyses are shown in Fig. 8. Rock-types in cyclic unit 7 are from base to top (Fig. 9):

pocC (troctolite). This consists of subhedral olivine crystals (1–3 mm; 30–59%), small, often euhedral chromites (<3%), plagioclase laths (<3 mm; 29–59%) and rare, dispersed Ca-rich pyroxene oikocrysts (<1 cm; 7–11%) (Fig. 7*a*). The modal proportion of plagioclase decreases upwards, and its shape changes from sub- and euhedral laths to resorbed anhedral grains. The olivine mode increases

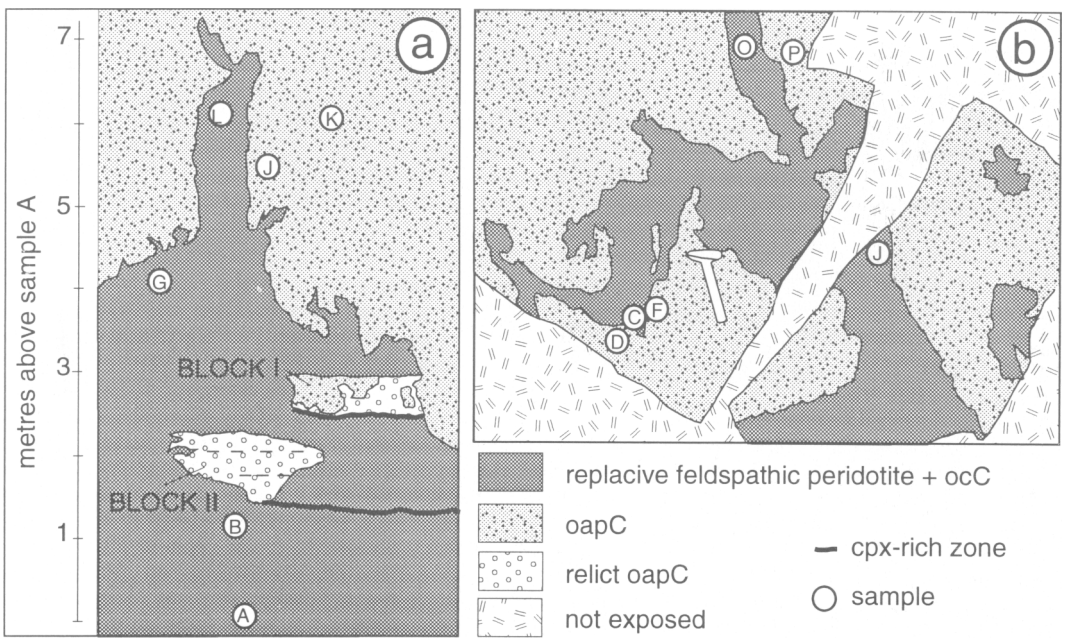

FIG. 6. Sketches showing details and sample locations in two selected localities along the ocC/oapC contact of cyclic unit 7. (*a*). Of the six samples (prefix H252) A is ocC; B, G and L are replacive peridotite and J and K are oapC. Two blocks of oapC floating in replacive peridotite can be used to illustrate the mechanisms of crystal–melt reaction. Block-I consists partly of almost totally replaced oapC and partly of oapC with layering parallel to the host. Block-II consists of almost totally replaced oapC with faint, just visible relict layering (plagioclase-rich bands) parallel to the host. A distinct, thin (<2 cm thick) zone enriched in Ca-rich pyroxene highlights the interface between partly replaced oapC and underlying, more mafic, replacive peridotite in some cases. Parts of this outcrop are believed to represent intermediate stages in the conversion of oapC to replacive peridotite. (*b*). (location is shown in Fig. 5). The location of six samples (prefix H207) is shown: C, J and O are replacive feldspathic peridotite while D, F and P are oapC.

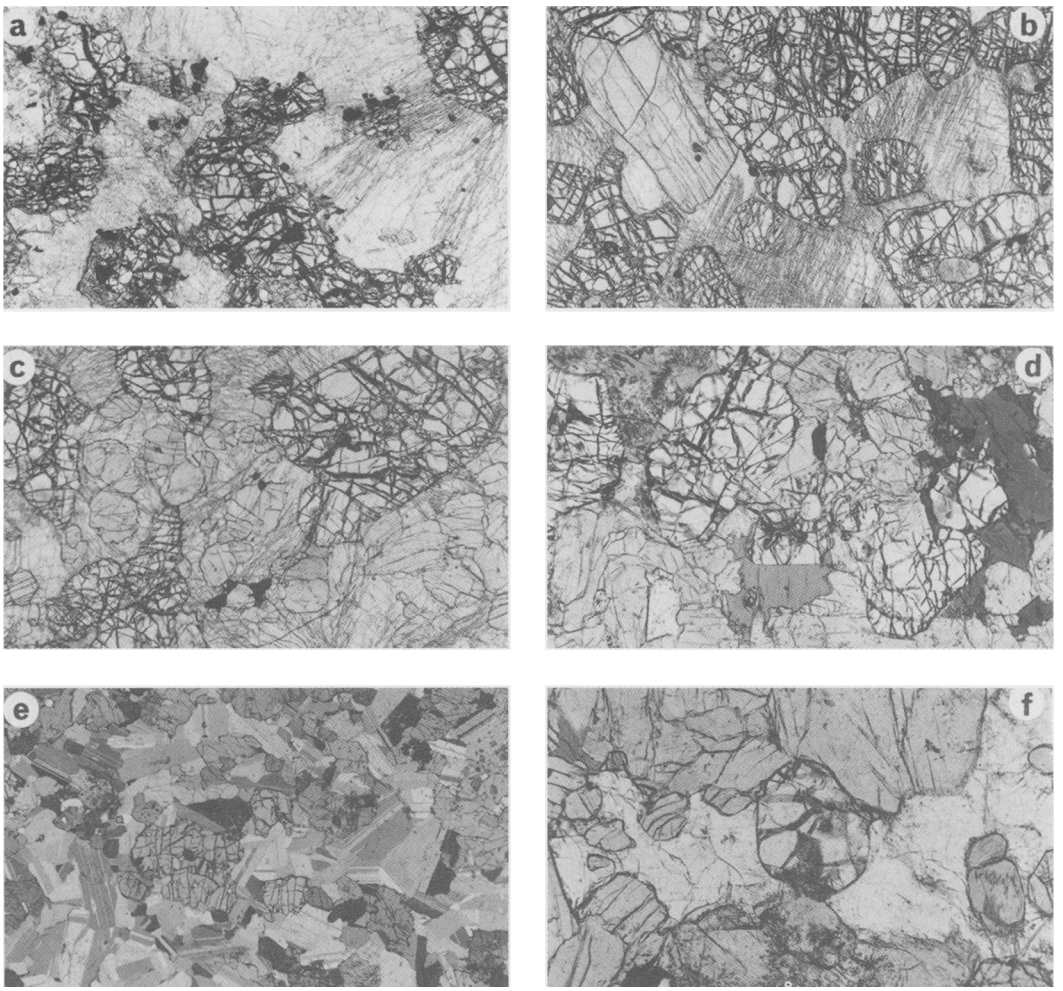

FIG. 7. Micro photographs showing typical textures of the main rock-types. Width of photos in *a*–*e* is ~6 mm. (*a*) pocC; (*b*) ocC. The amount of chromite in ocC is commonly higher than shown here. This photo shows one of the rare subhedral grains of Ca-rich pyroxene (upper left) suggesting a crystallization sequence of olivine/chromite-Ca-rich pyroxene-plagioclase in ocC; (*c*) oapC; (*d*) replacive peridotite. Note the presence of brown mica; (*e*) paoC; (*f*). Resorbed plagioclase in replacive peridotite. Width of photo is ~3 mm.

correspondingly until plagioclase forms oikocrysts, which is taken as the base of ocC.

ocC (peridotite/feldspathic peridotite). This rock type consists of rounded to euhedral olivines (1–4 mm, 68–78%) and small, dispersed (rarely within olivine), euhedral chromites (3–6%) within oikocrysts of Ca-rich pyroxene, plagioclase and sporadic Ca-poor pyroxene and phlogopite (Fig. 7*b*). In rare cases Ca-rich pyroxene occurs as subhedral, cumulus(?) grains, suggesting that the crystallization sequence is olivine–Ca-rich pyroxene–plagioclase. The texture and mineral modes (Fig. 8) suggest that ocC represents an olivine-chromite fractionate with plagioclase, Ca-rich and Ca-poor pyroxene having crystallized in cotectic proportions from trapped liquid.

oapC (olivine melagabbro). This contains more than 55% olivine + Ca-rich pyroxene and differs from the normal olivine gabbro (paoC) both texturally (Fig. 7*c*) and modally (Fig. 8). Olivines (1–3 mm; 27–55%) are subhedral; Ca-rich pyroxenes (22–42%) are slightly smaller (<2 mm), anhedral to subhedral and typically equant; phlogopite (<3%) is interstitial; plagioclase (19–42%)

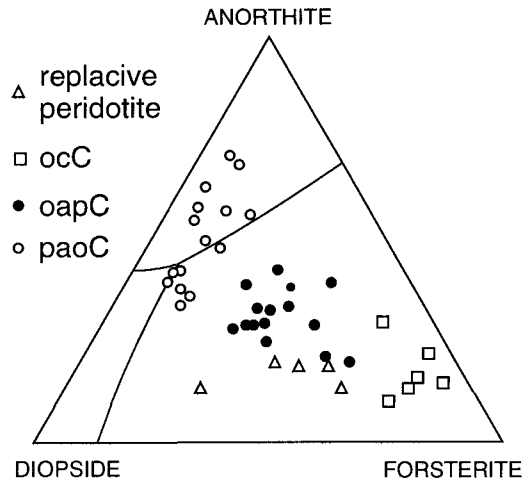

FIG. 8. The ternary forsterite–diopside–anorthite system (Morse *et al.*, 1987) showing point-counted mineral modes.

typically forms discrete, intercumulus or partly resorbed cumulus grains; Ca-poor pyroxene (2–10%) commonly forms large oikocrysts while euhedral chromite occurs in very small amounts (<5 grains per thin-section). The modal composition of oapC is clearly not cotectic (Fig. 8).

Replacive feldspathic peridotite. This is texturally very similar to oapC, but contains less plagioclase (Figs 7*d* and 8). Olivine forms subhedral, equant grains (22–56%; 1–3 mm) and Ca-rich pyroxene forms anhedral to subhedral, equant grains (26–43%; <2 mm). Ca-poor pyroxene megacrysts (2–19%) include anhedral olivine (often disaggregated into distinct grains with uniform extinction), Ca-rich pyroxene and a few plagioclase grains along their margins. This suggests that Ca-poor pyroxene megacrysts formed by reaction of cumulus minerals with trapped intercumulus liquid. Plagioclase (10–19%) grains either form anhedral grains showing evidence for resorption (Fig. 7*d,f*) or small oikocrysts including olivine and Ca-rich pyroxene. Small, subhedral to euhedral chromite and interstitial phlogopite may be present in small amounts.

paoC (olivine gabbro). This contains 29–71% plagioclase laths (<3 mm) forming a typical cumulus framework (Fig. 7*e*). Olivine (<2 mm; 4–18%) forms subhedral grains while some of the Ca-rich pyroxene (22–46%) occurs as subhedral, prismatic grains (up to 4 mm long), the rest being anhedral, equant grains comparable to those in the oapC. Chromite is not present and Ca-poor pyroxene is typically intercumulus, forming discrete interstitial grains or oikocrysts. Ca-poor pyroxene locally rims olivine and some of the Ca-poor pyroxene oikocrysts formed at the expense of resorbed Ca-rich pyroxene. The modal proportions are dispersed around the plagioclase-diopside-olivine cotectic (Fig. 8), and the paoCs are likely to represent a product of fractional crystallization.

Mineral chemistry

A total of ~800 new quantitative electron microprobe analyses were carried out as described by Tegner *et al.* (this volume). Representative mineral analyses are given in Table 1.

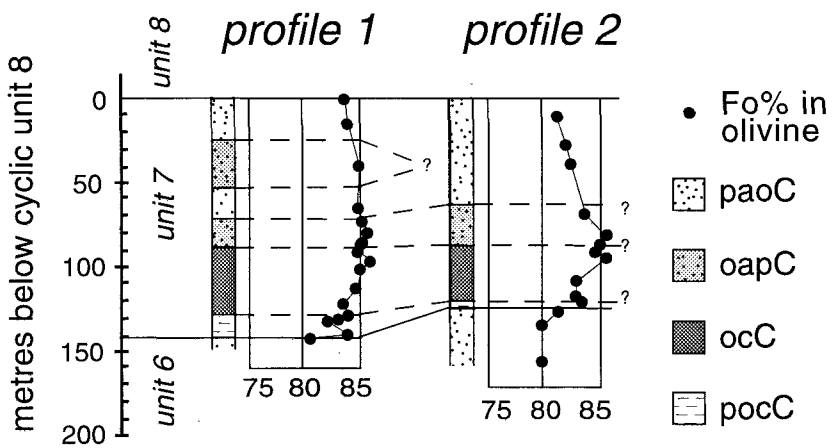

FIG. 9. Stratigraphic columns showing the lateral correlation of macrolayers in profiles 1 and 2 across cyclic unit 7. Cryptic variations of average Fo% in olivine (average of 6–9 analyses in each thin section) are shown to the right of the stratigraphic columns. 2σ deviations are <0.4 Fo% which is less than the size of the symbols.

TABLE 1. Representative electron microprobe mineral analyses from profile 1, Honningsvåg Intrusive Suite

sample no.	H120	H126	H207C	H144	H124	H127	H207C	H144	H124	H127	H207C	H144	H118	H207
rock-type	ocC	oapC	repl.peri.	paoC	ocC	oapC	repl.peri.	paoC	ocC	oapC	repl.peri.	paoC	ocC	repl.peri.
metres below cyclic unit 8	98	88	88	16	92	86	88	16	92	86	88	16	102	88
mineral	olivine	olivine	olivine	olivine	plag	plag	plag	plag	cpx	cpx	cpx	cpx	chrom	chrom
SiO_2, wt.%	40.15	39.87	38.84	39.44	48.21	47.89	46.12	46.67	51.66	52.68	51.21	52.36		b.d.
TiO_2									0.57	0.40	0.53	0.40	2.59	2.90
Al_2O_3					32.19	32.45	32.70	33.04	2.87	2.98	2.97	2.63	17.00	17.25
Cr_2O_3									1.13	0.80	1.13	0.64	37.21	38.19
FeO	12.97	13.96	14.72	14.88	0.12	0.13	0.08	0.17	4.40	4.85	4.35	4.53	33.29	29.98
MnO	0.19	0.19	0.18	0.21					0.12	0.10	0.14	0.15	0.39	0.31
NiO	0.20	0.23	0.22										0.11	0.18
MgO	46.95	45.66	46.90	45.44					18.16	18.64	17.49	18.32	7.48	9.07
CaO					15.39	15.63	16.33	16.72	19.46	18.96	21.04	20.33		
Na_2O					2.43	2.70	2.37	2.25	0.39	0.40	0.44	0.30		
K_2O					0.05	0.07	0.05	0.08						
Total	100.46	99.91	100.86	99.97	98.39	98.87	97.65	98.93	98.76	99.81	99.30	99.66	98.07	97.88
Mg#	86.6	85.4	85.0	84.5					88.0	87.3	87.8	87.8	29.2	41.5
An%					77.7	76.2	79.2	80.4						
formula based on:		4 oxygen atoms				8 oxygen atoms				6 oxygen atoms				4 oxygen
atoms														
Si	0.995	0.998	0.970	0.991	2.239	2.219	2.171	2.170	1.906	1.918	1.890	1.915		
Ti									0.016	0.011	0.015	0.011	0.064	0.071
Al					1.761	1.772	1.814	1.811	0.125	0.128	0.129	0.113	0.659	0.662
Cr									0.033	0.023	0.033	0.019	0.968	0.983
Fe	0.269	0.292	0.307	0.313	0.004	0.005	0.003	0.007	0.136	0.148	0.134	0.138	0.892	0.817
Mn	0.004	0.004	0.004	0.004					0.004	0.003	0.004	0.005	0.011	0.009
Ni	0.004	0.005	0.004										0.003	0.005
Mg	1.734	1.703	1.745	1.701					0.998	1.011	0.962	0.999	0.367	0.440
Ca					0.766	0.776	0.824	0.833	0.769	0.739	0.832	0.797		
Na					0.218	0.242	0.217	0.203	0.028	0.029	0.032	0.021		
K					0.003	0.004	0.003	0.005						
Total	3.006	3.002	3.030	3.009	4.991	5.018	5.032	5.029	4.015	4.010	4.031	4.018	2.964	2.987

b.d. = below detection limit (~0.05 wt.%); blank = not analysed; Mg# = 100Mg/(Mg+Fe); An% = 100Ca/(Ca+Na).

Cryptic variations in cyclic unit 7

The variations in olivine compositions (average Fo% of 6–9 analyses) across cyclic unit 7 in profile 1 and 2 are plotted in Fig. 9. The base of profile 1 is characterized by a compositional regression in olivine compositions from $\sim Fo_{81}$ at the top of unit 6 (paoC) to $\sim Fo_{86}$ ~35 m up in unit 7 ocC. Olivine compositions vary considerably within the pocC layer whereas the regression is smooth within ocC. The Fo % decreases slightly in the uppermost part of the ocC and then remains fairly constant (Fo_{85}) for the next ~50 m, hereafter it decreases slightly to $\sim Fo_{84}$ at the top of cyclic unit 7. It is worth noting that there are no discontinuities in Fo% between oapC and paoC macrolayers. The cryptic variation and composition of olivine in ocC in profile 2 mimics that of profile 1. In the upper part of profile 2, however, olivines evolve to more Fe-rich compositions (Fo_{81}). This is in accordance with the lateral variations shown to exist in paoC (Robins *et al.*, 1987; Tegner *et al.*, this volume).

Analyses of other minerals are not shown in Fig. 9 and can be summarized as follows: (1) the cryptic variation of Mg# in Ca-rich pyroxene mimics that of Fo% in olivine, though within a less significant compositional range (87–89); (2) the Cr_2O_3 content of chromites also mimics the Fo% curve with the least chromian samples at the base of the pocC sheet (~36 wt.% Cr_2O_3) and the most chromian values ~30 m up in the ocC (up to 42% Cr_2O_3) and (3) cumulus plagioclase compositions (An_{78-83}) show no systematic variations.

Mineral compositions in replacive peridotite and adjacent rocks

Olivines in replacive peridotite are generally slightly more Fe-rich (~1Fo%) than in adjacent ocC in profile 1 (Table 2). Chromites are slightly less chromian in replacive peridotite when compared to oapC and ocC; while plagioclase compositions cannot really be compared because of their texturally different habits.

Minor elements such as Cr and Ti in Ca-rich pyroxenes often provide valuable information about the composition of the magmas from which they crystallized. In this case the Mg# of Ca-rich pyroxene in all three rock-types is identical (Table 2) whereas significant variations can be seen in the Ti and Cr content (Fig. 10). The range of TiO_2 content in ocC and paoC is almost identical (~0.2–0.6 wt.%) whereas oapC (~0.2–1.2 wt.%) and replacive peridotites (~0.2–1.0 wt.%) have significantly higher values and cover a larger range. The Cr_2O_3 contents, on the other hand, show a large range of relatively low values in paoC (~0.0–1.0 wt.%) compared with a much narrower range of relatively high values in ocC (~1.0–1.3 wt.%). Replacive peridotites (~0.7–1.3 wt.%) and oapC (~0.2–1.4 wt.%) show a much larger range than in ocC, but reach the same high values.

Discussion

The origin of macrolayers of Intrusion II has previously been explained with a replenishment model (Fig. 2*a*). The formation of replacive fingers

TABLE 2. Average and variation compositions in replacive peridotite and adjacent rocks

rock type	replacive peridotite	oapC	ocC
no. of samples	5	7	4
Olivine			
Fo%, average	84.8	85.4	85.7
range	84.0–85.3	84.5–85.9	84.9–86.6
Clinopyroxene			
Mg#	88.0	88.3	88.1
range	86.1–89.4	86.3–89.7	87.2–89.2
Plagioclase			
An%, average	76.0	78.5	73.1
range	70.0–82.3	71.3–82.7	66.5–-77.9
Chromite			
Cr_2O_3 (wt.%)	37.0	38.5	39.0
range	36.4–38.2	37.9–39.7	37.2–42.1

Replacive feldspathic peridotite samples are: H207C, H207J and H207O; H252L and H252G
oapC samples are: H126; H127; H207D, H207F and H207P; H252K and H252J
peridotite (ocC) samples are: H118; H120; H124; H252A

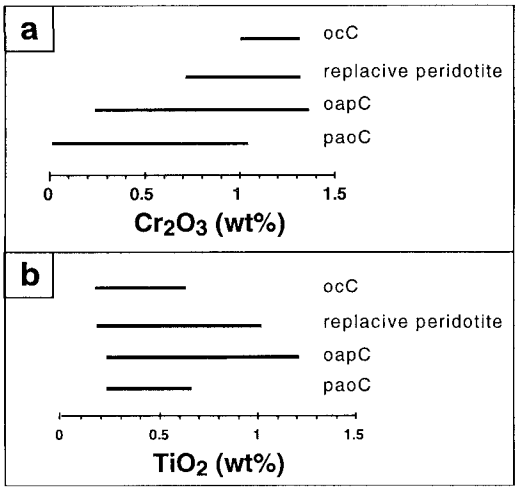

FIG. 10. Range of TiO_2 and Cr_2O_3 content in Ca-rich pyroxenes from the different rock-types in profile 1. Number of point analyses: ocC = 25; oapC = 89; paoC = 40; replacive peridotite = 30.

and pipes of feldspathic peridotite, in the replenishing model, have been ascribed to upward migration of pore magma within porous cumulates deposited from double-diffusive magma layers of different compositions (Robins *et al.*, 1987). An alternative interpretation for the upper part of Intrusion II is that the olivine-rich cumulates represent the products of crystal-melt reactions with intrusive picritic magma (Fig. 2*b*).

There is little doubt that the formation of cyclic units 1–5 is best explained with a replenishment model. First of all because the coupling between the step-like form of the base of the magma chamber and ocC macrolayers (Fig. 1, from Tegner *et al.*, this volume) is likely to be the result of episodic enlargement of the chamber during injections of new magma (Robins *et al.*, 1987). In the companion paper (Tegner *et al.*, this volume) it is also shown that cyclic units (consisting of paoC and pahC macrolayers) in the upper part of Intrusion II can be adequately explained in a replenishment model. Many aspects of the data presented above are consistent with both of the hypotheses (Fig. 2). A crucial point, however, is related to the crystallization sequence of the magma. In the replenishment model the magma has a crystallization sequence of olivine-plagioclase-Ca-rich pyroxene. The formation of replacive peridotite fingers and pipes mainly resulted from dissolution of plagioclase and crystallization of olivine by upwardly migrating pore magma. This is not compatible with the crystallization sequence of the replenishment magma; when Ca-rich pyroxene becomes saturated after plagioclase, dissolution of Ca-rich pyroxene should dominate over dissolution of plagioclase.

Replacive cumulates in Intrusion II

Magmatic replacement refers to postcumulus reaction between magma and cumulus minerals within a porous crystal framework (Irvine, 1982). The pipe and finger structures and the presence of oapC enclaves in replacive feldspathic peridotite (Figs 4–6) provide exceptionally strong evidence for the formation of peridotite as a consequence of crystal-melt reaction between host cumulates and migrating pore magma expelled upward from ocC. Several observations suggest that oapC sheets in cyclic unit 7 also resulted from crystal–melt reactions. (1) The non-cotectic modal proportions (Fig. 8) are unlikely to result from fractional crystallization. (2) The macrolayer sequence (ocC–oapC–paoC) is unlikely to result from progressive fractional crystallization. Phase diagram considerations in the anorthite–forsterite–diopside–silica system suggest that one must rely on the coincidence that the magma evolves from the olivine volume directly to a three-phase cotectic in order to explain the ocC/oapC transition. This is unlikely and therefore unsatisfactory in any crystallization model. (3) The resorbed (anhedral) nature of many plagioclases within oapC suggest crystal-melt reactions. (4) The large span in Cr-content of Ca-rich pyroxene within oapC (Fig. 10*a*), compared to ocC, suggests a mixed population spanning from relict paoC grains (low Cr-content), through partly equilibrated grains, to newly formed grains (high Cr-content). The same is the case for the feldspathic peridotite in replacive fingers and pipes. (5) The Ti-enrichment in many Ca-rich pyroxenes in oapC (and replacive peridotite), compared to paoC (Fig. 10*b*), suggest crystallization from, or reaction with, a relatively Ti-rich magma. Despite the Ti-poor compositions of Ca-rich pyroxenes in ocC, the incompatibility of Ti in Ca-rich pyroxene (Kd crystal/liquid = 0.4; Hart and Dunn, 1993) suggest that the Ti-content of expelled interstitial magma may be relatively high.

Crystal–melt reactions in layered intrusions

Crystal–melt reactions have been recognized in many layered intrusions as: (1) Modifications of mineral compositions resulting from reaction with migrating pore magma (e.g. Irvine, 1980). The term cryptic infiltration metasomatism has been proposed for this process (Irvine, 1982). (2) Modal changes which are most spectacular because one rock-type is replaced by another. Replacement in layered intrusions includes: the conversion of gabbro or troctolite

into peridotite (Robins, 1982; Butcher *et al.*, 1985; Tegner and Wilson, 1993); alteration of wehrlite, harzburgite, pyroxenite and olivine clinopyroxenite to dunite (Bennett *et al.*, 1986); transformation of gabbro or troctolite to anorthosite (McBirney and Sonnenthal, 1990; Boudreau and McCallum, 1992; Sonnenthal, 1992); troctolite converted into gabbro (Bédard *et al.*, 1988); anorthosite changed into clinopyroxenite (Tegner *et al.*, 1994); orthopyroxenite or norite converted into pegmatoidal feldspathic pyroxenite (Schiffries, 1982; Nicholson and Mathez, 1991; Mathez, 1995).

Modal changes result from reactant fluids resorbing minerals with which they are not saturated, and precipitating minerals in which they are saturated. The fluid may be: (i) migrating pore magma and/or vapour (e.g. Robins, 1982; Boudreau and McCallum, 1992; Tegner *et al.*, 1994; Mathez, 1995) expelled from underlying, porous cumulates; (ii) later magmatic intrusions (Bédard *et al.*, 1988; Tegner and Wilson, 1993); or (iii) chloride-rich solutions (Schiffries, 1982; Sonnenthal, 1992).

The replacive structures described here resemble the finger structures described in Norwegian and Scottish layered intrusions (Robins, 1982; Butcher *et al.*, 1985; Robins *et al.*, 1987). In these cases the finger formation has been ascribed to upward migration of magma expelled from a peridotitic cumulate into overlying porous troctolite or gabbro within a slowly solidifying layered series. The conversion of gabbro/troctolite to peridotite is ascribed to the assimilation of plagioclase and simultaneous precipitation of olivine (and Ca-rich pyroxene in some cases) by the migrating magma. The effect of elevated water content in the magma is believed to enhance the replacement process because it lowers both the density and the viscosity of the magma. Comparable replacive structures have also been described along contacts between wehrlite sills emplaced into olivine gabbro of the Kap Edvard Holm Complex, East Greenland (Tegner and Wilson, 1993). In this case replacive peridotite occurs both at the lower (dm–m sized fingers) and upper contacts of the sills (dm–m sized parasols), and where sills wedge out. Tegner and Wilson (1993) argued that overpressure within the intruding magma led to upward, downward and lateral migration of olivine-saturated magma into the surrounding, unconsolidated cumulates, causing crystal–melt reactions.

An alternative interpretation for the formation of finger structures has been proposed by Morse *et al.* (1987), who argued that the concordant peridotite layers on Rum crystallized from intrusive basaltic sills. The fingers represent dissolution structures caused by the upward transfer of latent heat released during crystallization of olivine within the sill. Subsequent crystallization and infilling of these structures resulted in peridotite fingers. The textural differences between ocC and oapC/replacive feldspathic peridotite described here argue against this interpretation.

Crystal–melt reactions in Intrusion II

The crystallization sequence is of fundamental importance to any crystal–melt reaction. Based on textural observations in ocC it is assumed that the intrusive magma was initially saturated in olivine alone (e.g. L_R in Fig. 11*a*) and follows a crystallization sequence of olivine–Ca-rich pyroxene–plagioclase. When migrating through a gabbroic crystal mush, L_R will evolve as a consequence of olivine precipitation ('-OL' arrow) and assimilation of gabbro ('+GAB' arrow) until the olivine–Ca-rich pyroxene cotectic is reached at L_W. Thereafter Ca-rich pyroxene co-precipitates with olivine in cotectic proportions (~86:14), and only plagioclase can be assimilated, driving the liquid towards the cotectic (L_{OG}) where the liquid is incapable of further assimilation because plagioclase is now a liquidus phase. The presence of phlogopite in ocC, oapC and replacive peridotite suggest the presence of some water. An elevated water content reduces the stability field of plagioclase relative to olivine and pyroxene (Yoder, 1965) and increases olivine stability relative to Ca-rich pyroxene (Kushiro *et al.*, 1968), hence the presence of water enhances the reactions described here.

Modifications in the proportion of crystals in the mush (the solid path) may be evaluated as follows. The point counted modes (Fig. 8) represent cumulus minerals and postcumulus overgrowth from trapped liquid. In order to eliminate overgrowths from trapped liquid (assumed to be 30% by volume), the modes have been recalculated to crystal modes in a porous mush containing 70% crystals and 30% cotectic liquid (Fig. 11*b*). Figure 11*b* shows that the conversion from a paoC to an oapC crystal mush required assimilation of plagioclase (−28% on average) and Ca-rich pyroxene (−10%), and crystallization of olivine (+38%). The conversion of oapC to replacive peridotite requires further assimilation of plagioclase (−20%) and crystallization of olivine (+13%) and Ca-rich pyroxene (+7%). In other words, rock conversion is mainly controlled by dissolution of plagioclase and crystallization of olivine. The role of Ca-rich pyroxene, that appears to be assimilated in some reactions and crystallizes in others, is explained by two solid paths as determined by the liquidus assemblage of the reactive magma. In olivine-saturated magma the solid path (#1) is controlled by crystallization of olivine ('+OL' arrow) and the assimilation of both plagioclase and Ca-rich pyroxene ('−GAB' arrow) as shown in Fig. 11*b*.

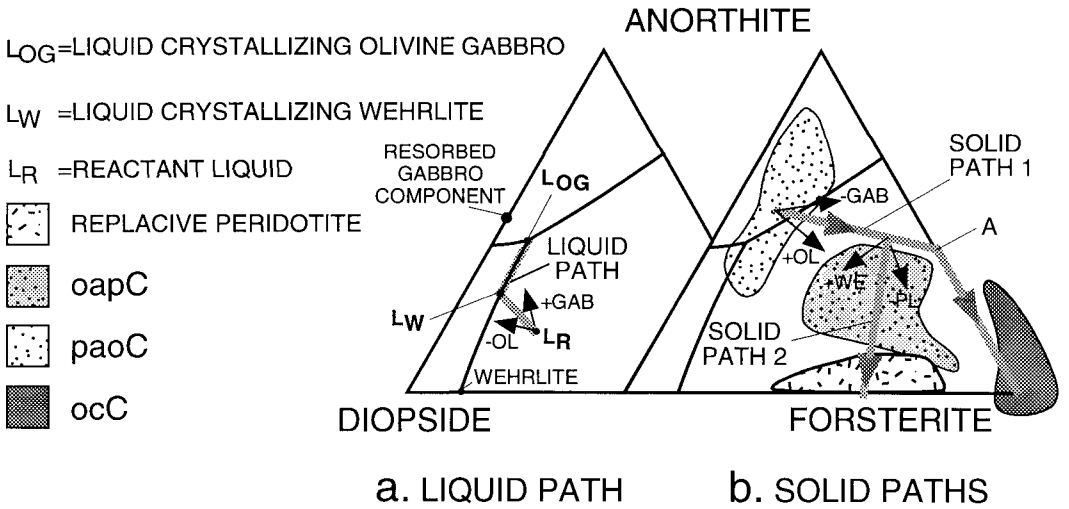

FIG. 11. Liquid and solid paths during crystal–melt reaction shown in the ternary forsterite–diopside–anorthite system (Morse *et al.*, 1987). See text for further explanation. In (*a*) the resorbed gabbro component is taken to have the ratio of Ca-rich pyroxene to plagioclase in oapC. In (*b*) the modal compositions are recalculated from the point-counted modes (Fig. 8) to mineral proportions in a crystal mush containing 70% crystals by subtracting 30% trapped magma of cotectic composition. The fact that the ocC field plots slightly outside the triangle illustrates that trapped liquid was less than 30% in this rock-type.

When the liquid is saturated with both Ca-rich pyroxene and olivine, the solid path (#2) is confined by the arrows indicating crystallization of wehrlite ('+WE') and assimilation of plagioclase ('−PL'). The arbitrary combination of reactions shown in Fig. 11*b* is just one of many paths that are capable of producing both oapC and replacive peridotite from paoC.

Two special cases should also be considered. Firstly, when a gabbroic crystal mush is continuously flushed by olivine-saturated magma. In this case crystal-melt reactions may lead to complete elimination of Ca-rich pyroxene at A (resulting in a troctolitic crystal mush) followed by elimination of plagioclase (resulting in an olivine crystal mush). The transitional pocC sheet below ocC in cyclic unit 7 is tentatively interpreted as a product of such a reaction. Secondly, when a non-reacted paoC mush initially is exposed to a reactant magma that precipitates Ca-rich pyroxene and olivine (solid path 2). In this case the end-product is a wehrlitic crystal mush (when plagioclase is eliminated, not shown). This reaction is likely to occur at the reaction front where the migrating magma, which has evolved to olivine and Ca-rich pyroxene saturation, enters unreacted mushes. The enrichment of Ca-rich pyroxene found in thin rims beneath relict rafts within ocC (Figs 4*e* and 6*a*) and in the persistent oapC layer within ocC (Fig. 3*d*) can be tentatively interpreted as representing preserved reaction fronts.

A two-stage model for Intrusion II

Any crystallization model for the upper part of Intrusion II should be able to account for all of the observations described here. In summary, this work has uncovered four significant features related to the olivine-rich rocks in and above cyclic unit 5: (1) some ocC sheets transgress paoC and pahC (Figs 1 and 3); (2) rafts and layers of gabbroic rocks occur within ocC (Figs 3*b–d*); (3) feldspathic peridotite fingers and pipes (Figs 4–6) are replacive; and (4) the oapC sheets have non-cotectic mineral assemblages and appear to result from crystal–melt reactions.

As described by Tegner and Wilson (1993), the emplacement of intracumulate sills in the Kap Edvard Holm Complex appears to be initiated by *lateral* infiltration of olivine-saturated magmas into porous cumulates. A similar process is envisaged in Honningsvåg. Continued addition of magma from a central feeder may lead to near complete assimilation of the host; this process gradually results in the development of a genuine picritic sill. Relict gabbroic rafts within ocC, and the lack of deformation of cumulates surrounding ocC sheets,

suggest that the space occupied by the sill partly resulted from assimilation of host rock and only partly by simple dilation. When lateral migration of magma ceased, solidification of the sill produced an ocC sheet. The development of fingers and pipes in the upper contact of the sill resulted from the release of relatively buoyant interstitial liquid during crystallization and compaction of ocC. Migration of three-phase saturated magmas may take place without leaving any petrographic evidence (Kerr and Tait, 1985; Robins *et al.*, 1987) and may account for the removal of components released during crystal–melt reactions (e.g. alumina).

The model of two-stage magmatism requires that picritic magmas were available after the formation of cyclic units. The geometry of the magma chamber, and the south-westward thinning of all olivine-bearing macrolayers (including cyclic units), suggest that magmas were generally fed into the central part of the Honningsvåg Intrusive Suite (to the NE of the described part of Intrusion II). This central region includes a possible feeder zone cutting Intrusion II (Robins *et al.*, 1987) that is likely to have fed magmas to Intrusions IV and V that developed by successive upward migration of magma chambers (Robins, 1993). Hence picritic magmas were available after deposition of the cyclic units of Intrusion II, as is evidenced by a dunitic plug found in the upper part of the suite (Robins *et al.*, 1987).

Conclusions

A two-stage intrusive model (Fig. 2*b*) may explain the cumulates and replacive rocks in the upper part of Intrusion II of the Honningsvåg Intrusive Suite.

Cyclic units crystallized from a magma with a crystallization sequence of olivine–plagioclase–Ca-rich pyroxene–Ca-poor pyroxene. Repeated magma replenishment events led to the development of cyclic units as described by Robins *et al.* (1987) and by Tegner *et al.* (this volume).

Later picritic sills (with a crystallization sequence of olivine–Ca-rich pyroxene–plagioclase) emplaced into still porous cumulates led to the formation of transgressive peridotite (ocC) sheets. Crystal–melt reactions when picritic magma infiltrated a porous, gabbroic host led to the formation of non-cotectic olivine melagabbro (oapC) sheets and replacive fingers and pipes of feldspathic peridotite.

Acknowledgements

CT acknowledges funding from the Danish Natural Science Research Council for a Ph.D. project carried out at the Geological Institute, University of Aarhus, and a research grant (to J. Richard Wilson) allowing field work. CT also acknowledges financial support from the Nordic Academy of Research and Education for a stay in Bergen during the course of this work. BR acknowledges the financial support of the Norwegian National Research Council. The Danish Research Council's funding of the Danish Lithosphere Centre is also acknowledged. Sidsel Grundvig is thanked for help with the microprobe work. The manuscript benefitted greatly from criticism on earlier versions by R. Grant Cawthorn, Henning S. Sørensen and J. Richard Wilson. A careful and helpful review by Michael Henderson is also appreciated.

References

Bédard, J.H. (1993) Oceanic crust as a reactive filter: Synkinematic intrusion, hybridization, and assimilation in an ophiolitic magma chamber, western Newfoundland. *Geology*, **21**, 77–80.

Bédard, J.H., Sparks, R.S.J., Renner, R., Cheadle, M.J. and Hallworth, M.A. (1988) Peridotite sills and metasomatic gabbros in the Eastern Layered Series of the Rhum complex. *J. Geol. Soc. Lond.*, **145**, 207–24.

Benn, K. and Laurent, R. (1987) Intrusive suite documented in the Troodos ophiolite plutonic complex, Cyprus. *Geology*, **15**, 821–4.

Bennett, M.C., Emblin, S.R., Robins, B. and Yeo, W.J.A. (1986) High-temperature ultramafic complexes in the North Norwegian Caledonides: I – Regional setting and field relationships. *Norwegian Geol. Surv. Bull.*, **405**, 1–40.

Bernstein, S., Rosing, M.T., Brooks, C.K. and Bird, D.K. (1992) An ocean-ridge magma chamber at a passive volcanic, continental margin: the Kap Edvard Holm layered gabbro complex, East Greenland. *Geol. Mag.*, **129**, 437–56.

Boudreau, A.E. and McCallum, I.S. (1992) Infiltration metasomatism in layered intrusions — An example from the Stillwater Complex, Montana. *J. Volcanol.*, **52**, 171–83.

Butcher, A.R., Young, I.M. and Faithfull, J.W. (1985) Finger structures in the Rhum Complex. *Geol. Mag.*, **122**, 491–502.

Girardeau, J. and Francheteau, J. (1993) Plagioclase-wehrlites and peridotites on the East Pacific Rise (Hess Deep) and the Mid-Atlantic Ridge (DSPD Site 334): evidence for magma percolation in the oceanic upper mantle. *Earth Planet. Sci. Lett.*, **115**, 137–49.

Hart, S.R. and Dunn, T. (1993) Experimental cpx/melt partitioning of 24 trace elements. *Contrib. Mineral. Petrol.*, **113**, 1–18.

Huppert, H.E. and Sparks, R.S. (1980) The fluid dynamics of a basaltic magma chamber, replenished by an influx of hot, dense, ultrabasic magma. *Contrib. Mineral. Petrol.*, **75**, 279–89.

Irvine, T.N. (1980) Magmatic infiltration metasomatism,

double-diffusive fractional crystallization, and adcumulus growth in the Muskox intrusion and other layered intrusions. In: *Physics of magmatic processes* (R. B. Hargraves, ed.), Princeton University Press, pp. 325–83.

Irvine, T.N. (1982) Terminology for layered intrusions. *J. Petrol.*, **23**, 127–62.

Juteau, T., Ernewein, M., Reuber, I., Whitechurch, H. and Dahl, R. (1988) Dualty of magmatism in the plutonic sequence of the Sumail Nappe, Oman. *Tectonophys.*, **151**, 107–35.

Kerr, R.C. and Tait, R. (1985) Convective exchange between pore fluid and an overlying reservoir of denser fluid: a post-cumulus process in layered intrusions. *Earth Planet. Sci. Lett.*, **75**, 147–56.

Kushiro, I., Yoder, H.S. and Nishikawa, M. (1968) Effect of water on the melting of enstatite. *Geol. Soc. Amer. Bull.*, **79**, 1685–92.

Mathez, E.A. (1995) Magmatic metasomatism and formation of the Merensky Reef, Bushveld Complex. *Contrib. Mineral. Petrol.*, **119**, 277–86.

McBirney, A.R. and Sonnenthal, E.L. (1990) Metasomatic replacement in the Skaergaard intrusion, East Greenland: Preliminary observations. *Chem. Geol.*, **88**, 245–60.

Morse, S.A., Owens, B.E. and Butcher, A.R. (1987) Origin of finger structures in the Rhum Complex: phase equilibrium and heat effects. *Geol. Mag.*, **124**, 205–10.

Nicholson, D.M. and Mathez, E.A. (1991) Petrogenesis of the Merensky Reef in the Rustenburg section of the Bushveld Complex. *Contrib. Mineral. Petrol.*, **107**, 293–309.

Renner, R. and Palacz, Z. (1987) Basaltic replenishment of the Rhum magma chamber: evidence from unit 14. *J. Geol. Soc. Lond.*, **144**, 961–70.

Robins, B. (1982) Finger structures in the Lille Kufjord layered Intrusion, Finnmark, Northern Norway. *Contrib. Mineral. Petrol.*, **81**, 290–95.

Robins, B. (1993) The evolution of the Honningsvåg Intrusive Suite, Magerøy, Northern Norway. *Norwegian Geol. Soc. Geonytt*, **93**, (abstract).

Robins, B., Gading, M., Yurdakul, M. and Aitcheson, S.J. (1991) The origin of macrorhythmic units in the Lower Zone of the Lille Kufjord Intrusion, northern Norway. *Norwegian Geol. Surv. Bull.*, **420**, 13–50.

Robins, B., Haukvik, L. and Jansen, S. (1987) The organization and internal structure of cyclic units in the Honningsvåg Intrusive suite, North Norway: Implications for intrusive mechanisms, double-diffusive convection and pore-magma infiltration. In: *Origins of Igneous Layering*, (I. Parsons, ed.), Reidel, pp. 287–312.

Schiffries, C.M. (1982) The petrogenesis of a platiniferous dunite pipe in the Bushveld Complex: infiltration metasomatism by a chloride solution. *Econ. Geol.*, **77**, 1439–53.

Sonnenthal, E.L. (1992) Geochemistry of dendritic anorthosites and associated pegmatites in the Skaergaard Intrusion, East Greenland: Evidence for metasomatism by a chlorine-rich fluid. *J. Volcanol.*, **52**, 209–30.

Tegner, C. and Wilson, J.R. (1993) A late ultramafic suite in the Kap Edvard Holm layered gabbro complex, east Greenland. *Geol. Mag.*, **130**, 431–42.

Tegner, C., Wilson, J.R. and Cawthorn, R.G. (1994) The dunite-clinopyroxenite pegmatoidal pipe, Tweefontein, eastern Bushveld Complex, South Africa. *Sth. Afr. J. Geol.*, **97**, 415–30.

Tegner, C., Robins, B. and Sørensen, H.S. (1996) Crystallization from stratified magmas in the Honningsvåg Intrusive Suite, Northern Norway: A reappraisal. *Mineral. Mag.*, **60**, 41–51.

Wager, L.R. and Brown, G.M. (1968) *Layered Igneous Rocks*. Oliver and Boyd, London, 588 pp.

Yoder, H.S. (1965) Diopside-anorthite-water at five and ten kilobars and its bearing on explosive volcanism. *Carnegie Inst. Washington Yearbk.*, **64**, 82–9.

[*Revised manuscript received 10 July 1995*]